JACS
JOURNAL OF THE AMERICAN CHEMICAL SOCIETY
Article
pubs.acs.org/JACS

Ligand-Dependent Activation and Deactivation of the Human Adenosine A_{2A} Receptor

Jianing Li,[†] Amanda L. Jonsson,[†] Thijs Beuming,[‡] John C. Shelley,[§] and Gregory A. Voth*[,†]

[†]Department of Chemistry, Institute for Biophysical Dynamics, James Franck Institute and Computation Institute, The University of Chicago, 5735 South Ellis Avenue, Chicago, Illinois 60637, United States

[‡]Schrödinger, Inc., 120 West 45th Street, 17th Floor, New York, New York 10036, United States

[§]Schrödinger, Inc., 101 Southwest Main Street, Suite 1300, Portland, Oregon 97204, United States

Supporting Information

ABSTRACT: G-protein-coupled receptors (GPCRs) are membrane proteins with critical functions in cellular signal transduction, representing a primary class of drug targets. Acting by direct binding, many drugs modulate GPCR activity and influence the signaling pathways associated with numerous diseases. However, complete details of ligand-dependent GPCR activation/deactivation are difficult to obtain from experiments. Therefore, it remains unclear how ligands modulate a GPCR's activity. To elucidate the ligand-dependent activation/deactivation mechanism of the human adenosine A_{2A} receptor (AA2AR), a member of the class A GPCRs, we performed large-scale unbiased molecular dynamics and metadynamics simulations of the receptor embedded in a membrane. At the atomic level, we have observed distinct structural states that resemble the active and inactive states. In particular, we noted key structural elements changing in a highly concerted fashion during the conformational transitions, including six conformational states of a tryptophan ($Trp246^{6.48}$). Our findings agree with a previously proposed view that, during activation, this tryptophan residue undergoes a rotameric transition that may be coupled to a series of coherent conformational changes, resulting in the opening of the G-protein binding site. Further, metadynamics simulations provide quantitative evidence for this mechanism, suggesting how ligand binding shifts the equilibrium between the active and inactive states. Our analysis also proposes that a few specific residues are associated with agonism/antagonism, affinity, and selectivity, and suggests that the ligand-binding pocket can be thought of as having three distinct regions, providing dynamic features for structure-based design. Additional simulations with AA2AR bound to a novel ligand are consistent with our proposed mechanism. Generally, our study provides insights into the ligand-dependent AA2AR activation/deactivation in addition to what has been found in crystal structures. These results should aid in the discovery of more effective and selective GPCR ligands.

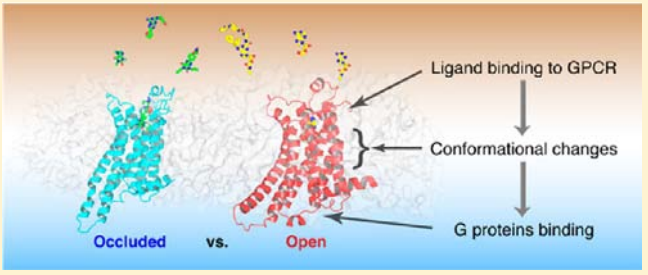

INTRODUCTION

G-protein-coupled receptors (GPCRs) are membrane proteins critical for the sense of sight, smell, and taste as well as for movement and mood regulation.[1] They exist in equilibrium between inactive and active states, but only in the active state can they couple with G-proteins and trigger signal transduction. This equilibrium can be shifted upon ligand binding, regulating the activity of the GPCR. Because of their important physiological roles and implications in numerous diseases,[2−4] GPCRs represent a primary class of therapeutic targets, with many projects seeking small-molecule ligands as potential drug candidates.[5−7] Therefore, it is essential to understand the ligand-triggered activation and deactivation of GPCRs. X-ray crystallography has provided the structures of several GPCR−ligand complexes, all of which are members of class A, the largest GPCR subgroup. In addition to the well-known heptahelical framework, all the class A GPCR crystal structures have a ligand-binding site that is distant from the G-protein binding site. Ligand binding induces local changes that are propagated through the receptor to the G-protein binding site, likely involving a coherent mechanism.[8] However, while crystallography provides snapshots of the GPCR states, little is currently known about the dynamic process of these conformational changes. Although technologies like fluorescence resonance energy transfer (FRET) and site-directed spin labeling (SDSL) are able to monitor conformational changes of some key residues,[9−12] direct experimental tracking of these coherent conformational changes is generally difficult to achieve. Crucial dynamic details, such as how ligands induce specific conformational changes of GPCRs and how these changes influence the association with G-proteins, are still unclear in the overall picture of GPCR activation. Knowledge about these details should aid in the development of effective and selective GPCR ligands via structure-based design

Received: May 2, 2013
Published: May 16, 2013

dx.doi.org/10.1021/ja404391q | J. Am. Chem. Soc. 2013, 135, 8749−8759

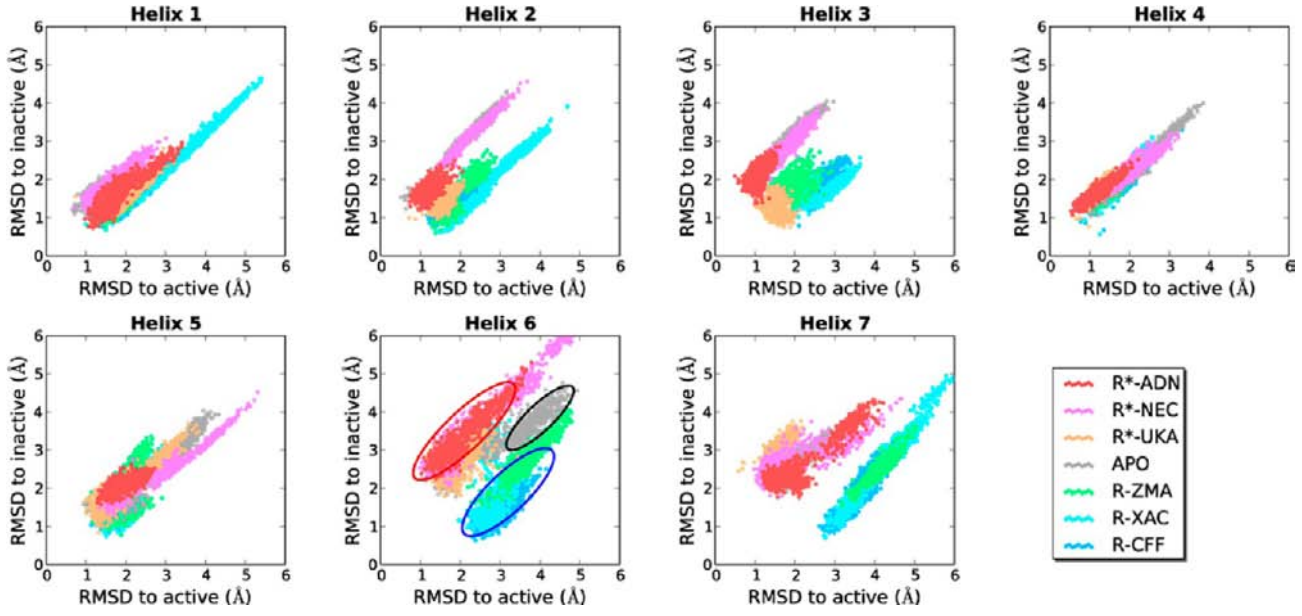

Figure 1. C_α RMSDs of the seven transmembrane helices to the active and inactive crystal structures (PDB IDs: 3QAK and 3REY). For helix 6, as a guide to the eye, the three distinct regions are highlighted by red (agonist-bound), black (apo), and blue (inverse-agonist-bound) ellipses. We determined the positions and shapes of the ellipses by maximizing the inclusion of points from the target state while minimizing the inclusion of points from the other states. In addition to the distinct states in TM6, the RMSDs of helix 7 also display two distinct states corresponding to agonist-bound/apo and inverse-agonist-bound complexes.

approaches. Thus, elucidating these details from computational studies could be very valuable.

In this work, we study the ligand-dependent activation and deactivation of an important GPCR—the adenosine A_{2A} receptor (AA2AR)—a typical class A GPCR and an emerging drug target.[13] Previous simulations of rhodopsin and adrenergic receptors[14−18] have revealed general backbone movements that result from ligand binding but also suggested some notable differences in the activation mechanism for individual GPCRs. It remains controversial how the various proposed conformational changes are coupled. Indeed, whether there is a "general" activation/deactivation mechanism for all GPCRs remains an open question. Recently, a small number of studies employing molecular dynamics (MD) have provided some information on the dynamic aspects of AA2AR conformations that cannot be inferred from the currently available crystal structures.[19−22] However, the mechanism of ligand-dependent activation and deactivation for AA2AR has never been fully discussed, and an examination of the ligand-specific impacts on both the structure and the free energy landscape of AA2AR has also not been reported.

GPCR activity is modulated by ligands generally classified as (partial or full) agonists, neutral antagonists, and inverse agonists. When an agonist is bound, the aforementioned equilibrium is shifted toward the active state, which can couple with G-proteins (in the case of AA2AR, G_s and G_{olf}). Dissociation of G_s or G_{olf} subsequently induce an increased level of the second messenger, cyclic adenosine monophosphate (cAMP), which in turn triggers a complex sequence of events leading to various cellular responses.[13] On the contrary, when an inverse agonist is bound, the equilibrium is shifted toward the inactive state. As a consequence, AA2AR fails to couple with G_s or G_{olf}, impeding the signal transduction. Neutral antagonists bind to the receptor and act by blocking the site. Although formally this classification stipulates that they do not affect the equilibrium between the active and inactive states, most of them in fact are weak agonists or inverse agonists.[23] Recently, ligands of AA2AR have been extensively studied as drug candidates for the treatment of ischemic, coronary artery, and inflammatory diseases as well as Parkinson's disease and drug-induced movement disorder.[24−28]

Both agonist- and inverse-agonist-bound AA2AR complexes have been crystallized, providing a suitable data set for us to study the ligand-dependent activation and deactivation of AA2AR *in silico*. Using multiple ligand-bound AA2AR models, we therefore performed extensive unbiased MD and metadynamics simulations to address two major questions: (1) what are the fundamental structural and energetic differences between the active state and the inactive state; (2) how do the various ligands affect the equilibrium between these states?

■ RESULTS AND DISCUSSION

Our starting models were prepared from crystal structures of AA2AR. During our modeling, all the mutations were reverted to the wild-type sequence with a short C-terminus (residues 1−325, the longest AA2AR construct available in the Protein Data Bank). At the outset of this work (at the end of 2011), structures had been determined for seven AA2AR complexes with six different organic ligands, namely, the endogenous agonist adenosine (ADN), the synthetic full agonists NECA (NEC) and UK-432097 (UKA), the inverse agonist ZM-241385 (ZMA), and the xanthine-based antagonists xanthine amine congener (XAC) and caffeine (CFF) (Table S1, Supporting Information). The last two ligands are actually found to act as inverse agonists during pharmacological characterization.[29] We also included in our data set a new, nonribose partial agonist LUF5834 (LUF).[30,31] Generally, these ligands span a wide range of activities and sizes, but all are assumed to bind to the same pocket. From the crystal structures, we constructed AA2AR models in a solvated membrane model to provide a realistic environment. In the rest of this work, we use R* to represent a receptor model that

dx.doi.org/10.1021/ja404391q | J. Am. Chem. Soc. 2013, 135, 8749−8759

was constructed from a crystal structure originally bound to an agonist and R to represent a model constructed from a crystal structure originally bound to an inverse agonist. We have carried out large-scale MD simulations, totaling over 10 μs, on 12 systems: six systems of AA2AR bound to the cocrystallized ligands (R*-ADN, R*-NEC, R*-UKA, R-ZMA, R-XAC, and R-CFF), one apo system, two systems with adenosine and LUF in an AA2AR structure originally bound to ZMA (R-ADN and R-LUF), and two systems with ZMA and caffeine, respectively, in an AA2AR structure originally bound to adenosine (R*-XAC and R*-CFF), as well as one model system of AA2AR complexed with the C-terminus (residues 380–394) of the G_s alpha subunit ($G_{\alpha s}$).

Simulations Reveal Three Conformational States for Transmembrane Helix 6 (TM6). The transmembrane helices generally move as rigid bodies with relatively flexible ends in our unbiased MD simulations. To understand the dynamics of each transmembrane helix, we have carried out structural comparisons of the conformations we sampled to two crystal structures that are considered to be in the active and inactive states, respectively (PDB IDs: 3QAK and 3REY). With global superimposition of the C_α atoms, root-mean-square deviations (RMSDs) are calculated for C_α atoms in each transmembrane helix (Figure 1). The large range of RMSDs indicates that a variety of conformational ensembles have been visited, some quite distinct from the crystal structures. Among all the helices, TM6 not only demonstrates the most significant changes with the widest range of RMSDs (2–8 Å) but also clearly shows three distinguishable conformational states. While TM6 adopts the active-state-like conformations with the bound agonists, it also adopts the inactive-state-like conformations with the bound inverse agonists. However, without any ligand, TM6 adopts a separate state intermediate between the active and inactive states.

To quantify the conformational changes of TM6 induced by different ligands, we first examined the helical distortion around Pro248$^{6.50}$ (the superscript of the residue refers to the Ballesteros–Weinstein numbering[32]). Often described in terms of kink and wobble angles,[33] the proline-induced distortion in TM6 has been suggested to propagate the ligand-binding conformational changes to the transmembrane region of GPCRs.[34,35] Comparing the agonist-bound conformations to the inverse agonist-bound ones that we sampled, TM6 has, on average, a 10% larger average kink angle but a 8% smaller average wobble angle in the former, showing that TM6 is more likely to adopt an outward conformation with agonists (Figure S1, Supporting Information). The wide distributions of these angles also highlight the plasticity of TM6 in complexes containing agonists. In the apo simulation, TM6 displays the largest average kink and wobble angles, which indicates a separate state from the ligand-bound ones. The outward movement of TM6 is also captured by the increased distance between TM3 and TM6 in the agonist-bound simulations (calculated using the positions of the C_α atoms of Arg102$^{3.50}$ and Ala232$^{6.34}$, Figure S1, Supporting Information). Thus, the average distance is 9.7 Å with agonists, 7.3 Å without ligands, and 7.2 Å with inverse agonists. These distances remain consistent with those in the crystal structures of AA2AR (9.5 Å with agonist UKA[36] and 6.7 Å with inverse agonist ZMA[37]). However, they are smaller than those observed in the crystal structures of the β2-adrenergic receptor (14.1 Å with an agonist[38] and 8.4 Å with an inverse agonist[39]), leaving an open question whether the intracellular crevice of AA2AR is sufficiently open.

Since a G-protein binds to the intracellular crevice surrounded by multiple helices,[40,41] a single distance measurement between a helical pair is not enough to characterize how open the G-protein binding site is. The active conformation of a GPCR should have a cavity large enough to accommodate the relevant portion of the G-protein, which appears to correspond to the five terminal residues of $G_{\alpha s}$ based upon the examination of the crystal structure of the β2-adrenergic receptor–G_s protein complex.[41] We calculated an average active binding site volume of 804 ± 76 Å^3 from the equilibrated portion of a simulation of an AA2AR–$G_{\alpha s}$ complex (Figure S2, see the Supporting Information text for details). As an approximation, we define conformations with volumes greater than 800 Å^3 as open while those with volumes less than that as occluded. The trajectories from the various ligand–protein complexes were then analyzed to determine the average G-protein binding site volume and fraction of open conformations sampled (see Figure 2).

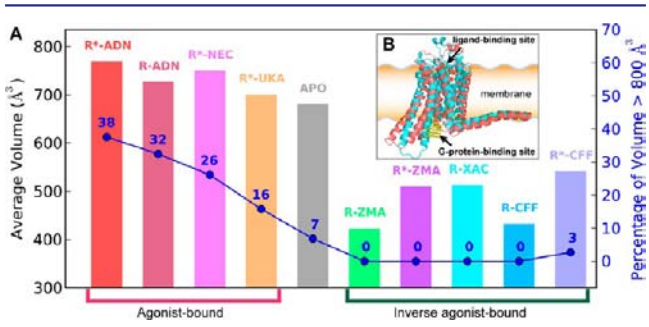

Figure 2. Volume of the G-protein binding site in AA2AR simulations: (A) Graph of the average volume (bars, left scale) of the G-protein binding site and the fraction of conformations with volume greater than 800 Å^3 (plot, right scale), calculated from the longest trajectory of each system. (B) A cartoon to illustrate our definition of the G-protein binding site. An example of the superimposed open and occluded conformations (red and cyan) is shown. These two conformations were snapshots from the longest simulations of R*-ADN and R-XAC taken at 350 ns. The yellow dots indicate the space needed to accommodate the terminal helix of $G_{\alpha s}$.

Opening of the G-Protein Binding Site Could Be Fundamental for GPCR Activation. We found three distinct combinations of the fraction of open conformations and average volume, as shown in Figure 2:

(1) a large average volume (~700–800 Å^3) in the agonist-bound simulations and a comparatively large fraction of conformations with volume greater than 800 Å^3
(2) a large average volume in the apo simulations (~600–700 Å^3) but a small fraction of conformations with volume greater than 800 Å^3
(3) a small average volume (~350–550 Å^3) in the inverse agonist-bound simulations and very few or no conformations with volume greater than 800 Å^3

In good agreement with the nature of the bound ligands, the trends reported here indicate the propensity of the receptor to undergo conformational changes necessary for G-protein binding, even though the open conformations do not guarantee coupling. Generally, the average volumes suggest that agonist binding induces the G-protein binding site to open, while inverse agonist binding induces it to contract. As almost no

dx.doi.org/10.1021/ja404391q | J. Am. Chem. Soc. 2013, 135, 8749–8759

open conformations were sampled, the G-protein binding site remains occluded during our inverse agonist-bound simulations. In contrast, our agonist-bound and apo simulations sampled significantly more open conformations. It is noteworthy that the agonist-bound simulations show an average distance of 10.9 Å between TM3 and TM5 (Figure S1, Supporting Information), compared to those of 9.5 and 9.1 Å in the active-state crystal structures of AA2AR and the β2-adrenergic receptor, respectively. Hence, even though the intracellular ends of TM3 and TM6 are not very far apart, an increase in the TM3−TM5 separation contributes here to the opening of the G-protein binding site in our agonist-bound simulations. Further, while our data demonstrate that the volume of the intracellular crevice provides a good approximation to distinguish agonist-bound AA2ARs from those inverse-agonist-bound ones, it appears poorly correlated with the relative potency of these agonists. Below we try to address the challenge of agonist ranking with metadynamics simulations, pertaining to a key residue in the activation process. In addition, the apo AA2AR simulations have reduced open conformations compared to the agonist-bound ones (as low as 18−44%), even though the system was derived from an agonist-bound structure (PDB ID: 2YDO). It is tempting to suggest that the remainder of open conformations, which appear infrequently during the entire apo simulation (Figure S3A, Supporting Information), correlates with the "basal activity" of AA2AR observed in *in vitro* experiments.[29,42] Interestingly, prior experiments have shown that truncation of the C-terminus reduces the basal activity of AA2AR: while removal of the sequence after residue 360 (residues 1−360) results in a slightly decreased basal activity, further truncation of the C-terminus (residues 1−311) shows a very significant decrease.[43] Our apo model of the wild-type AA2AR contains residues 1−325, which includes the conserved and structurally important part of helix 8, and therefore represents a variant between the aforementioned two.

As shown in Figure 2, the opening of the G-protein binding site is associated with agonists only. This is most clearly demonstrated by the simulations, which were started from constructs built from crystal structures by replacing the original ligands with those of the opposite efficacy (e.g., agonist ligands replacing inverse agonists and vice versa). We found that the results for a given ligand were very similar, regardless of the starting receptor conformation. For example, the G-protein binding site opens upon placement of adenosine into the structure originally bound to ZMA (R-ADN), with the average volume and fraction of open conformation close to those of adenosine in the cocrystallized structure (R*-ADN). On the other hand, the opening of G-protein binding site is greatly reduced with the agonist adenosine replaced by the inverse agonists ZMA (R*-ZMA) and caffeine (R*-CFF). Such observations are consistent with earlier FRET experiments, in which agonist-induced conformational changes were reversed after addition of a saturating concentration of inverse agonist and vice versa.[44,45] Furthermore, comparing the simulations starting from the same AA2AR structure with an agonist and an inverse agonist, respectively, we observe the opposite behaviors in the G-protein binding site (Figure S3, Supporting Information). Such ligand dependence not only shows a high consistency with respect to the ligand efficacy but also highlights the effectiveness of the simulations, which seem capable of eliminating bias from the initial constructs.

Conformational Changes of Key Structural Elements Are Coupled to the Opening of the G-Protein Binding Site. Along with the modulation in the opening of the G-protein binding site, we have observed differences between active and inactive states in several structural elements of AA2AR, including (1) a separation between the intracellular ends of TM3 and TM5/TM6, (2) a rearrangement of the salt bridge network, (3) side chain rearrangement in the transmembrane core, and (4) rotameric transitions of Trp246$^{6.48}$. First of all, the intracellular ends of TM3 and TM6 are shifted ∼2 Å further apart in the active state than in the inactive state (Figure 3A and Figure S1, Supporting Information) which is

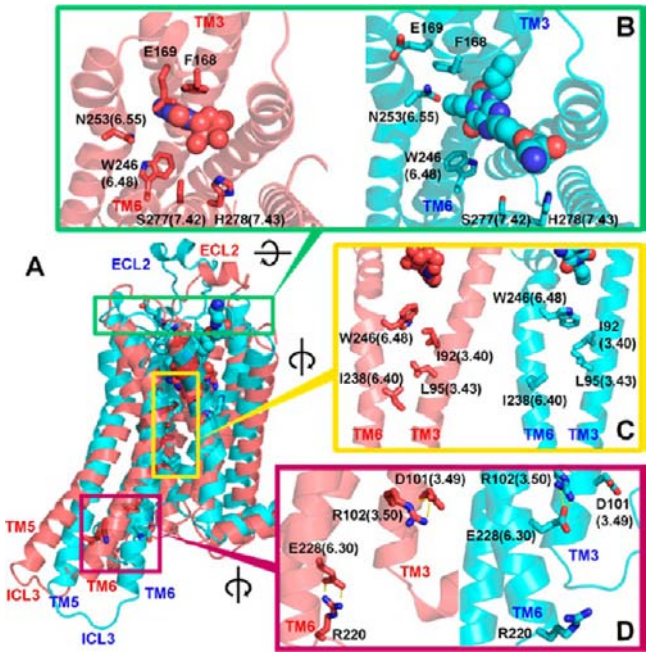

Figure 3. Comparison of the key structural elements in the active (red) and inactive (cyan) conformations from simulations of R*-ADN and R-XAC, respectively. (A) Superposition of two snapshots at 350 ns. (B) Ligand−AA2AR interactions. The ligand is shown using a space-filling representation. (C) Trp246$^{6.48}$ and key residues involved in the packing between TM3 and TM6. (D) The salt bridge network.

consistent with the experimental hypothesis that increased separation of the intracellular ends of TM3 and TM6 opens up the G-protein binding site.[46] Along with the separation of TM3 and TM6, there is a 1−2 Å outward movement of TM5 in the intracellular ends (Figure S1, Supporting Information). Second, we noticed that the broken so-called ionic lock (the salt-bridge between Arg102$^{3.50}$−Glu228$^{6.30}$ thought to be a hallmark of the inactive state[47]) and increased separation of TM3 and TM6 are coupled, consistent with what was observed in rhodopsin and β2-adrenergic receptor.[46,48] We also found that, when the ionic lock is not present, alternative salt bridges such as Arg102$^{3.50}$−Asp101$^{3.49}$ and Arg220$^{6.22}$−Glu228$^{6.30}$ can form (Figure 3D). These alternative salt bridges seem to be stable enough to prevent the ionic lock from forming again. In addition, the alternative salt bridge Arg220$^{6.22}$−Glu228$^{6.30}$ induces intracellular loop 3 (ICL3) to adopt more compact conformations (Figure 3A). We speculate that, while rearrangement of the salt bridge network impacts the opening of the G-protein binding site directly, it might also affect the association with G_s

dx.doi.org/10.1021/ja404391q | J. Am. Chem. Soc. 2013, 135, 8749−8759

indirectly by allowing the tighter contacts between AA2AR and G_s.

It is also apparent that side-chain rearrangement in the transmembrane core correlates with the rotameric transition of Trp246$^{6.48}$. For example, along with the reoriented Trp246$^{6.48}$ in the active conformation, the contacts between Ile92$^{3.40}$/Leu95$^{3.43}$ and residues in TM6 are disrupted, while the entire side chain of Ile238$^{6.40}$ is rotated more than 60° (Figure 3C). To further clarify the preferred rotameric states of Trp246$^{6.48}$, we analyzed the distribution of two side-chain dihedrals χ1 and χ2 throughout the simulation (Figure 4). The nonoverlapping

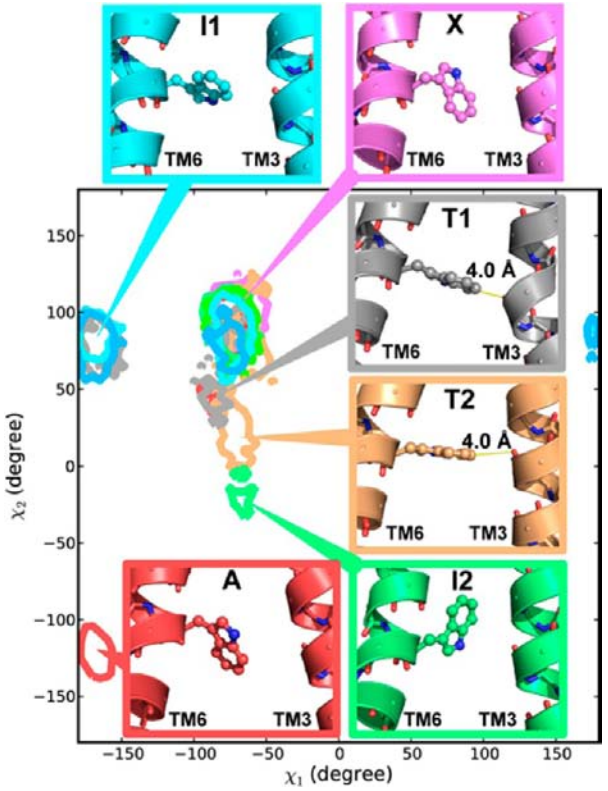

Figure 4. Trp246$^{6.48}$ χ1 and χ2 distributions and their representative conformations. The regions enclosed by the contour lines have a normalized probability higher than 0.005. The shortest heavy atom distance between the Trp246$^{6.48}$ side chain and the TM3 backbone is labeled for the states T1 and T2. Table S2 contains the details of each simulation regarding the fraction of time spent in each rotameric state. The original scatter plot is shown as Figure S5 (Supporting Information). The color scheme is consistent with Figure 2.

regions in Figure 4 represent six distinct conformational sets, which we labeled as rotameric states X, T1, T2, I1, I2, and A (namely, X for the state in crystals, T1 and T2 for transient intermediate states, I1 and I2 for the inactive states, and A for the active state). Overall, the simulations bound to agonists and inverse agonists sampled distinct distributions of rotameric states, with the exception of state X, which is visited in all simulations. Aside from state X, there are clear correlations between the type of ligand and the rotameric states of Trp246$^{6.48}$. Agonists visit states T1, T2, and A, while inverse agonists visit states I1 and I2. These results suggest that state A is only allowed after activation and that states I1 and I2 are associated with the inactive state. Notably, in the short-lived state T1 or T2, the indole ring of Trp246$^{6.48}$ stays perpendicular and close to TM3 (4.0 Å between the closest heavy atoms), and our interpretation of the data indicates that they are intermediate states for AA2AR activation (see the Supporting Information text for details).

It is noteworthy that the populated regions of the tryptophan side chain dihedrals shown in Figure 4 are also found in a recent PDB survey of tryptophan residues (Figure S5C, Supporting Information),[49] indicating that the conformations of the six states that we identified are accessible in many native protein structures. The finding of multiple Trp246$^{6.48}$ rotameric states not only agrees with the previously proposed view that a rotameric transition is involved in GPCR activation[8] but also further advances the activation model built from prior studies of rhodopsin[50] and adrenergic receptors.[17] Both χ1 and χ2 are necessary to characterize the rotameric states of Trp246$^{6.48}$, while the majority of previous studies only focused on χ1[19,51] except in a recent simulation of the serotonin 5-HT$_{2A}$ receptor.[52] χ1 or χ2 has been employed as one collective variable in earlier metadynamics studies of GPCRs;[51,53] however, little attention is devoted to both of them. To the best of our knowledge, this is the first analysis of both tryptophan χ1 and χ2 rotation for GPCR activation in atomic detail. Since some of these rotameric states were induced only by a subset of ligands, a full mapping of the accessible dihedral space required the study of a broad data set of ligands, something only possible recently thanks to the increasing number of GPCR crystal structures. In addition, these large-scale simulations also allow capturing states that either are short-lived (i.e., states T1 and T2) or appear after a long simulation only (i.e., state A).

AA2AR Activation and Deactivation Mechanism. Herein we propose a possible mechanism for AA2AR activation based on our unbiased MD simulations and provide quantitative support for this mechanism from metadynamics simulations. First, following direct contact with an agonist, Trp246$^{6.48}$ is forced to undergo a side chain rotation that causes crowding in the transmembrane core. To release this congestion, adjacent side chains have to rearrange. The rearrangement is gradually extended to the intracellular side as the original hydrophobic packing of many residues, such as Ile92$^{3.40}$, Leu95$^{3.43}$, and Ile238$^{6.40}$, is disrupted. As a result, interactions between TM3 and TM6 are greatly weakened, allowing TM6 to move away from TM3 while breaking the ionic lock. At the same time, TM5 also moves away from TM3. The increased separation between TM3 and TM5/TM6 then causes the G-protein binding site to open. The entire process, especially the side chain rearrangement, can be visualized as a "domino effect" where the initial "push" comes from the agonist entering the ligand-binding site.

On the other hand, the mechanism of AA2AR deactivation seems to be much simpler, as fewer conformational changes are involved. Relative to the apo state, an inverse agonist causes AA2AR to contract the helical bundle, as evidenced by the shorter distances between TM3 and TM6 on both the extracellular and cytoplasmic sides of the membrane. This contraction, in turn, leads to tighter ligand binding and a collapse of the G-protein binding site, which prompts the formation of the ionic lock. Although in some AA2AR crystal structures the distance between the inverse agonist and Trp246$^{6.48}$ can be as close as 4.2 Å, our simulations show that the inverse agonists fail to cause the rotation of Trp246$^{6.48}$ to the rotameric states associated with activation. Instead, Trp246$^{6.48}$ adopts conformations associated with the inactive

dx.doi.org/10.1021/ja404391q | J. Am. Chem. Soc. 2013, 135, 8749−8759

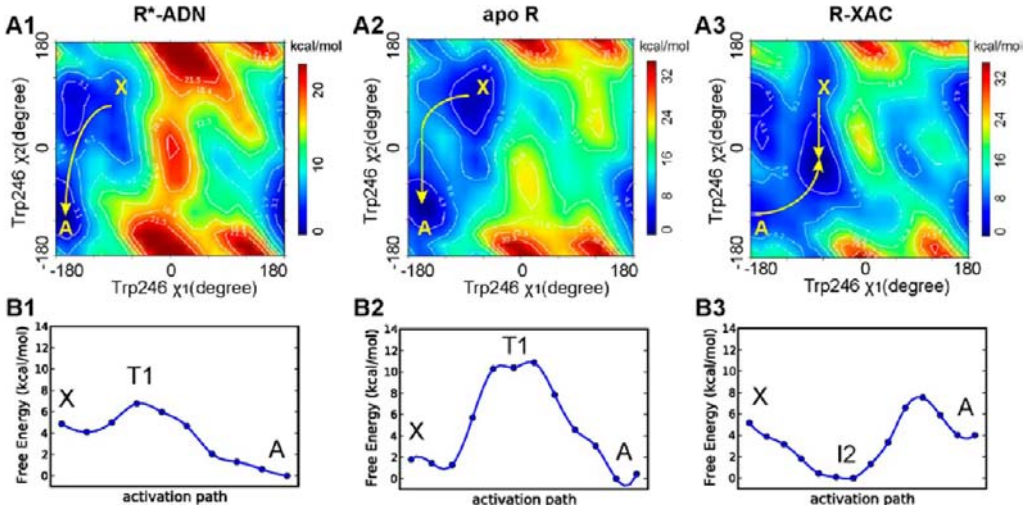

Figure 5. Metadynamics results of R*-ADN, apo-R, and R-XAC simulations. (A1−3) The free energy surface as a function of Trp246$^{6.48}$ dihedral angles χ1 and χ2. (B1−3) The minimum free-energy path between states X and A.

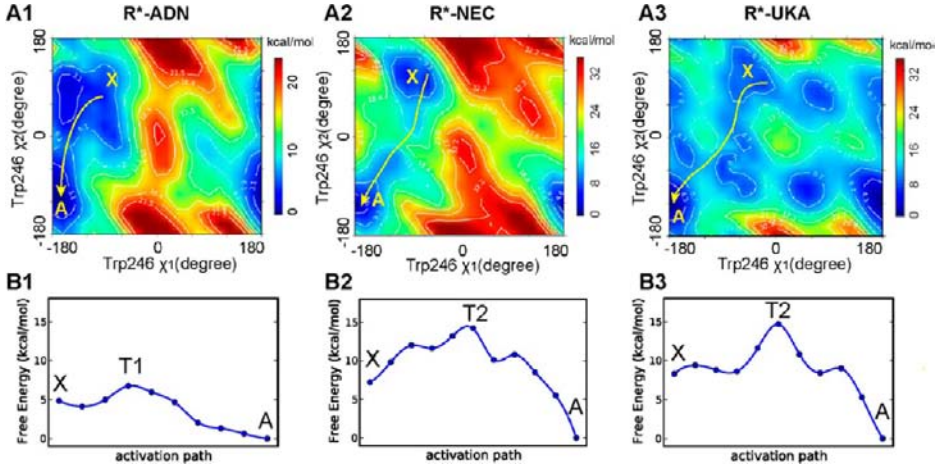

Figure 6. Metadynamics results of R*-ADN, R*-NEC, and R*-UKA simulations. (A1−3) The free energy surface as a function of Trp246$^{6.48}$ dihedral angles χ1 and χ2. (B1−3) The minimum free-energy path between states X and A.

states, along with enhanced packing inside the transmembrane core.

As Trp246$^{6.48}$ rotation seems to be key for activation, we carried out metadynamics simulations using its χ1 and χ2 as collective variables. Metadynamics is an enhanced free energy sampling method that is capable of exploring infrequent events and mapping out the free energy surface of the selected variables.[54] Our results are presented in Figure 5 for three simulations: (1) with the agonist adenosine, (2) with no ligand, and (3) with the inverse agonist XAC. The resulting free energy landscapes are considerably modified by the presence and efficacy of ligands. The ligand-free free-energy landscape shows two potential wells centered at states X and A. The lowest free-energy value for state A is 1.8 kcal/mol lower than that for state X, but the activation barrier between these states is 10.2 kcal/mol (Figure 5B2). When adenosine binds, the overall free energy landscape is similar except that the activation barrier is substantially decreased by 7.4 kcal/mol and state A is 4.9 kcal/mol more favorable than state X, a difference that is 3.1 kcal/mol larger than for the ligand-free state (Figure 5B1). Therefore, it seems clear that agonist binding not only lowers the activation barrier but also increases the stability of the active state, so that the active state is promoted both kinetically and thermodynamically. In contrast, XAC modifies the free-energy landscape so that it contains two completely different basins—the I1 and I2 states. Our results (Figure 5B3) suggest that state I2 is the most favorable state and has a considerably lower free energy than both states X and A. This thermodynamic/energetic argument explains how the inverse agonist shifts the equilibrium to an inactive conformation, resulting in overall deactivation of AA2AR.

The free-energy profiles of Trp246$^{6.48}$ with three different agonists are compared in Figure 6. Although adenosine has the lowest barrier among the three agonists we studied (2.8, 7.0, and 6.4 kcal/mol for adenosine, NEC, and UKA, respectively), our metadynamics analysis shows that its free-energy difference from state A to X is only 4.9 kcal/mol, which is 2.3 and 3.4 kcal/mol smaller than that of NEC and UKA, respectively (7.2 and 8.3 kcal/mol). Since the order of the free-energy differences seems to be consistent with the rank of potency (assessed as EC50 in experiments), we investigated the correlation between those two properties quantitatively with a linear regression analysis. We found a correlation coefficient (r^2) of 0.98 for correlating the logarithm of EC50 with our calculated free-energy differences (Figure S6, Supporting Information). Thus, our small data set suggests that

dx.doi.org/10.1021/ja404391q | J. Am. Chem. Soc. 2013, 135, 8749−8759

Table 1. Comparison of Ligand–Residue Interactions[a]

AA2AR residues		agonists			inverse agonists		
		ADN	NEC	UKA	ZMA	XAC	CFF
Lower Region	Trp246$^{6.48}$ [b]	20	9	8			
	Thr88$^{3.36}$ [c]	58 (82)	73 (91)	100 (100)	0 (1)	0 (6)	0 (4)
	Asn181$^{5.42}$ [c]	42 (73)	2 (15)	10 (41)	2 (5)		
	Ser277$^{7.42}$ [c]	30 (63)	33 (56)	100 (100)			0 (8)
	His278$^{7.43}$ [c]	20 (83)	64 (94)	99 (100)	0 (5)		0 (31)
Middle Region	Val84$^{3.32}$ [d]	76	83	100	72	97	90
	Leu85$^{3.33}$ [d]	78	89	100	89	77	59
	Phe168$^{5.29}$ [e]	94	71	100	100	72	96
	Glu169$^{5.30}$ [c]	34 (83)	19 (75)	1 (39)	51 (93)	0 (23)	4 (37)
	Met177$^{5.38}$ [d]	65	57	97	87	89	45
	Leu249$^{6.51}$ [d]	61	80	100	100	75	48
	His250$^{6.52}$ [e]	2			97		
	His250$^{6.52}$ [c]	53 (95)	3 (30)	54 (86)	22 (39)	5 (19)	6 (13)
	Asn253$^{6.55}$ [c]	38 (87)	26 (79)	6 (18)	100 (100)	80 (95)	88 (94)
	Ile274$^{7.39}$ [d]	21	78	100	98	70	44
Upper Region	Ser6$^{1.30}$ [c]			18 (26)	5 (8)	0 (2)	
	Tyr9$^{1.33}$ [c]	1 (9)	10 (65)	85 (94)	0 (3)	1 (24)	
	Ile10$^{1.34}$ [d]			43		1	
	Glu13$^{1.37}$ [c]	2 (8)	7 (76)	20 (72)	0 (2)	6 (10)	0 (1)
	Ala63$^{2.61}$ [d]	18	57	82	3	88	75
	Ile64$^{2.62}$ [d]			43		1	
	Ile66$^{2.64}$ [d]	10		21	10	98	89
	Ser67$^{2.65}$ [c]	46 (83)	33 (88)	58 (91)	7 (78)	47 (80)	4 (48)
	Thr68$^{2.66}$ [c]			6 (8)			
	Leu267$^{7.32}$ [d]			81	64	76	
	Met270$^{7.35}$ [d]	10	24	100	95	79	43
	Tyr271$^{7.36}$ [c]		2 (19)	9 (50)	45 (48)	4 (24)	0 (1)

[a]Percentages of time that the interactions formed are reported using the longest trajectory for each complex. [b]Close contact: distance between one heavy atom in the ligand and one heavy atom in the Trp246$^{6.48}$ side chain within 3.6 Å. A relatively short cutoff was chosen here to reflect the unusually close contacts, approximated to the sum of van der Waals radii for two CH groups. [c]Polar contact: We define a direct contact if the distance from one N or O atom in the ligand to one N or O atom in the protein side chain is within 4.2 Å; the indirect contact is defined if the distance between the two closest polar atoms is greater than 4.2 Å, but there is at least one water molecule that forms hydrogen bonds (heavy atom distance <4.2 Å) to both atoms. The number in parentheses represents the percentage of time with either direct or indirect contact. [d]Nonpolar contact: distance from a nonpolar atom in the ligand to another nonpolar atom in the side chain within 5.0 Å. The nonpolar atoms are defined as heavy atoms with partial charges whose absolute values are less than 0.30 electron unit. [e]$\pi-\pi$ stacking contact: distance between the centers of the aromatic core in the ligand and the aromatic side chain within 6.5 Å. The cutoff was chosen to include both the parallel and T-shape $\pi-\pi$ interactions.

metadynamics simulations can not only distinguish agonists from inverse agonists but may also provide a potential theoretical assessment for AA2AR agonist potency.

Three Regions in the Ligand-Binding Pocket. Despite the availability of crystal structures for a number of GPCR–ligand complexes, the current understanding of the relationship between ligand positioning and interactions with residues in the binding pocket with the activation process is still limited. By identifying the key AA2AR–ligand interactions, we can provide a dynamic view of AA2AR–ligand interactions to complement the static information from the crystal structures. As presented in Table 1, the residue–ligand interactions are analyzed and categorized into three distinct regions in the binding pocket in accordance with prior experimental studies.[31,55,56] We then relate the propensity of certain residue–ligand interactions to agonism/antagonism, affinity, and selectivity. We believe such information will be beneficial for structure-based design of AA2AR ligands.

Lower Region. As shown in Table 1, only agonists can approach Trp246$^{6.48}$ and form close contacts with that residue, which is consistent with our proposed mechanism. In addition, the polar contacts to Thr88$^{3.36}$, Asn181$^{5.42}$, Ser277$^{7.42}$, and His278$^{7.43}$ differentiate agonists from inverse agonists. Interestingly, despite the direct contacts to these residues exhibited in crystal structures, we found that indirect contacts, mediated by water molecules, also play an import role in the agonist-bound simulations. Our data suggests that these residues, together with the surrounding water molecules, compose a hydrogen-bonding network that stabilizes the binding of the adenosine-derived agonists. Indeed, some of the water molecules have been captured in crystal structures.[57] The importance of this polar network is supported by previous mutagenesis studies, in which the Thr88Ala, Asn181Ala, and Ser277Ala mutants all lead to a reduction of agonist affinity.[58,59] In addition, the lack of persistent interactions between XAC and Thr88$^{3.36}$/Ser277$^{7.42}$ in our simulations is in agreement with the lack of effect on XAC binding of the Thr88Ala and Ser277Ala mutants.[58,59] It is difficult, however, to explain why the His278Ala mutant loses its specific binding with both agonists and inverse agonists/antagonists,[59] solely based on the

dx.doi.org/10.1021/ja404391q | J. Am. Chem. Soc. 2013, 135, 8749–8759

presence of persistent direct or water-mediated interactions observed in our simulations. In this case, it is conceivable, that—in addition to the disruption of the hydrogen-bonding networks—the impact of the mutation may well be passed along to a number of neighboring residues, such as Glu13$^{1.39}$ and Ile274$^{7.39}$, which have persistent interactions with His278$^{7.43}$ (52 and 97% of time in the R-XAC simulation). In addition, our results support a hypothesis by Kim and co-workers,[59] which states that His278$^{7.43}$ displays various interactions to other residues and could be essential in maintaining AA2AR conformations. Both our simulations and mutagenesis evidence suggest a complicated role for His278$^{7.43}$ mutations in the loss of ligand binding. Moreover, it has been found that, with high concentrations of agonists, the mutants Ser277Ala and His278Ala still display full stimulation of cAMP production.[59] Indeed, there are almost no polar and nonpolar contacts (<5% of time) between Trp246$^{6.48}$ and Ser277$^{7.42}$/His278$^{7.43}$ in our simulations, and the conformational properties of Trp246$^{6.48}$ should be unaffected by the aforementioned mutations.

Middle Region. The $\pi-\pi$ stacking between Phe168$^{5.29}$ and the ligands' aromatic cores (e.g., adenine or xanthine moieties) is present over 70% of the time in all simulations, suggesting that such $\pi-\pi$ interactions are important for binding of all the ligands studied here. Our data provide good agreement with prior experiments,[56] which found that mutation of Phe168$^{5.29}$ to alanine abolished the binding of both agonists and antagonists while mutation to tyrosine/tryptophan had only a subtle effect.

Furthermore, the five hydrophobic residues Val84$^{3.32}$, Leu85$^{3.33}$, Leu249$^{6.51}$, Met177$^{5.38}$, and Ile274$^{7.39}$ were found to interact with the ligands in 20−100% of time. All ligands interact with Val84$^{3.32}$, which agrees with the prior finding that the mutations Val84Ala and Val84Asp eliminate specific agonist/antagonist binding.[60] Although both Leu249$^{6.51}$ and Met177$^{5.38}$ consistently interact with the ligands, the Leu249Ala mutation affects both agonist and antagonist binding, while Met177Ala affects binding of antagonist ZMA but not agonist NEC.[56] We explain this difference by comparing the number of nonpolar contacts of these residues with the ligands: Leu249$^{6.51}$ on average has 2−6 contacts with all the ligands we studied, in contrast to Met177$^{5.38}$, which interacts tightly with ZMA (3.3 average contacts) but loosely with NEC (1.4 average contacts).

Moreover, Glu169$^{5.30}$ and Asn253$^{6.55}$ interact with the ligands by either direct or indirect polar contacts. Indeed, the Glu169Gln mutant displays an ∼20-fold decrease in its NEC binding affinity.[61] On the other hand, we found that Glu169$^{5.30}$ did not interact with XAC directly, consistent with earlier mutagenesis data that mutation to glutamine has no effect to XAC binding.[61] Compared to Glu169$^{5.30}$, Asn253$^{6.55}$ displays a tighter interaction with all the ligands in our simulations, consistent with the loss of binding for both agonists and antagonists observed in mutants such as Asn253Ala, Asn253Ser, and Asn253Gln.[59] It is also noteworthy that Asn253$^{6.55}$ is bound to all the inverse agonists in over 80% of time, while the water-mediated contact (although not shown in Table 1) forms in almost 100% of time, suggesting a crucial hydrogen-bonding network near Asn253$^{6.55}$ for inverse agonists.

Prior experiments found that mutations of His250$^{6.52}$ affect the ligand binding in a complicated fashion: while the His250Phe and His250Tyr mutations have only modest effects on NEC binding to AA2AR, His250Ala significantly disrupts binding of both NEC and XAC.[59] Surprisingly, our simulations demonstrate neither $\pi-\pi$ stacking nor hydrogen bonding between His250$^{6.52}$ and NEC/XAC. However, the many conformations sampled in our simulations suggest that bulkier aromatic side chains can be tolerated at residue 250, without disrupting the aromatic cluster formed among Phe182$^{5.43}$, His250$^{6.52}$, and Trp246$^{6.48}$, which apparently compensates for the loss of water-mediated polar contacts between His250$^{6.52}$ and Asn253$^{6.55}$ (formed over 50% of time in R*-NEC and R-XAC simulations, also found in crystal structures 2YDV and 4EIY). On the other hand, the loss of ligand binding in the His250Ala mutant[59] is possibly due to the dual loss of the integrity of the aromatic cluster as well as the water-mediated polar contacts.

Upper Region. Interestingly, the residues mentioned above are mostly conserved among different adenosine receptors (subtypes A_1, A_{2A}, A_{2B}, and A_3), so that the ligand-binding pockets of these subtypes share many similarities in the lower and middle regions. This has led to the previous proposition[56] that the selectivity of ligands for the adenosine receptor subtypes is mediated by the upper region encompassed by TM1, 2, and 7, which is more diverse among different receptor subtypes. While there are several conserved residues in this region that interact with all ligands (such as Tyr9$^{1.33}$, Glu13$^{1.37}$, Ala63$^{2.61}$, Ile64$^{2.62}$, Ile66$^{2.64}$, Ser67$^{2.65}$, and Tyr271$^{7.36}$), UKA, ZMA, and XAC also interact with several nonconserved residues. ZMA and UKA selectively bind to the A_{2A} subtype,[62,63] and XAC has a slight selectivity for the A_{2A} subtype.[64] Despite their different sizes and structures, these selective ligands differ from the others studied here by their unique interactions with Ser6$^{1.30}$, Leu267$^{7.32}$, and Met270$^{7.35}$. In addition to the cases we tested, two new AA2AR crystal structures of A2A specific inhibitors (PDB IDs: 3UZA and 3UZC) also display the same interactions, in particular with Met270$^{7.35}$.[65]

On the basis of the analysis of persistent interactions between AA2AR and the ligands in our MD simulations as well as the mechanism we propose, we divide the ligand-binding site into three regions (Figure 7): the lower region (Trp246$^{6.48}$, Thr88$^{3.36}$, Asn181$^{5.42}$, Ser277$^{7.42}$, and His278$^{7.43}$), the middle region (Val84$^{3.32}$, Leu85$^{3.33}$, Phe168$^{5.29}$, Glu169$^{5.30}$, Met177$^{5.38}$,

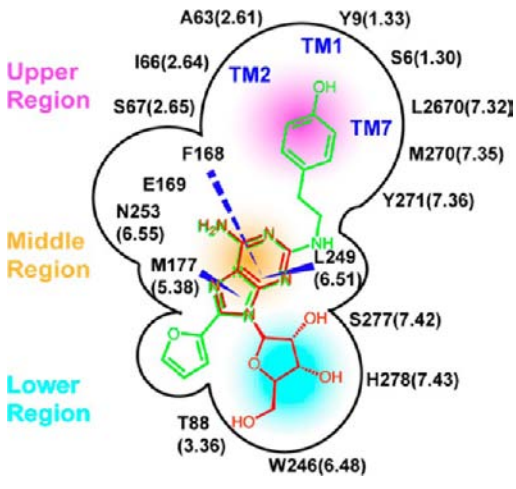

Figure 7. Cartoon of the ligand-binding pocket projected into two dimensions. The chemical structures of the endogenous agonist adenosine (red) and the selective inverse agonist ZM-241385 (green) are superimposed by overlapping the adenine ring and the triazolotriazine ring.

dx.doi.org/10.1021/ja404391q | J. Am. Chem. Soc. 2013, 135, 8749−8759

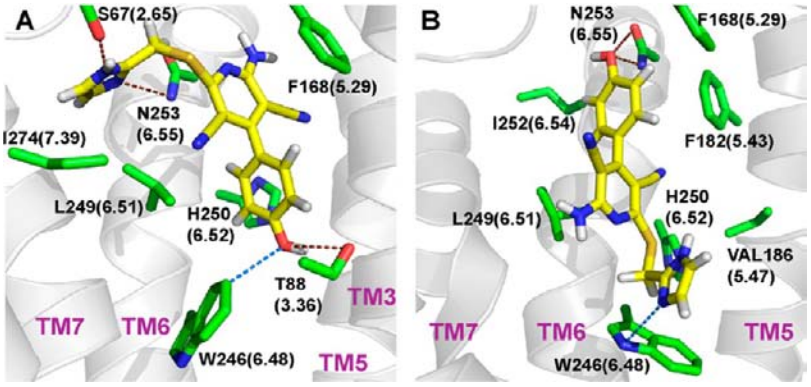

Figure 8. Snapshots of AA2AR–LUF contacts when LUF approaches Trp246$^{6.48}$. Part A is from 74 ns into the first simulation, while part B is from 150 ns into the second simulation. The brown dashed lines represent hydrogen bonds, while the blue ones represent the LUF–Trp246$^{6.48}$ closest contacts within 4.4 Å.

Leu249$^{6.51}$, His250$^{6.52}$, Asn253$^{6.55}$, and Ile274$^{7.39}$), and the upper region (a number of residues from TMs 1, 2, and 7). Our interpretation of the available information suggests a fairly simple overall characterization based upon the nature of the protein–ligand interactions in each of the three regions in the binding site, namely, that the lower region determines agonism/antagonism, the middle region is key for binding affinity, and the upper region is likely related to the subtype selectivity. Different from earlier works based on crystal structures or mutagenesis,[31,56] our interpretation is based on the dynamics aspects of the wild-type AA2AR–ligand–solvent interactions. Therefore, our simulations not only add knowledge of the ligand dynamics beyond the crystal structures but also provide useful hints to aid the design of effective and selective ligands for the AA2AR receptor.

Simulations with a New Ligand Confirm Our Proposed Mechanism. In order to validate the proposed AA2AR activation mechanism, we simulated a novel agonist LUF, which contains neither an adenine nor a ribose moiety, as our test case. Since there are no available crystal structures for the AA2AR–LUF complex, we designed two possible poses of LUF based on the three regions of the ligand-binding pocket, and replaced the cocrystallized ligand in an inactive-state crystal structure (PDB ID: 3EML) with both models (see the Supporting Information text for detail). One simulation was performed with each model. The first simulation started with an LUF pose in which the hydroxyphenyl group resides in the lower region of the pocket (Figure 8A). Through the simulation, the pyridine core of LUF forms a stable $\pi-\pi$ stacking with Phe168$^{5.29}$, as well as hydrophobic contacts to Leu249$^{6.51}$, possibly contributing to the high affinity of LUF to AA2AR.[33] The hydroxyl group forms hydrogen bonds with Thr88$^{3.36}$ and His250$^{6.52}$, as does the imidazole group with Ser67$^{2.65}$ and Asn253$^{6.55}$. Contacts are found between the hydroxyphenyl group and Trp246$^{6.48}$ in the lower pocket shortly. The binding mode found in this simulation is consistent with mutagenesis experiments, in which mutation of Phe168$^{5.29}$ or Asn253$^{6.55}$ to alanine greatly reduced the activity of AA2AR modulated by LUF.[31] The second simulation contains an alternate binding mode, in which the imidazole group is oriented toward the lower region (Figure 8B). We observed that, in this binding mode, the hydroxyphenyl group forms an aromatic cluster with the side chains of Phe168$^{5.29}$ and Phe182$^{5.45}$, while the imidazole group forms a T-shape packing to Trp246$^{6.48}$. Except for hydrogen bonding to Asn253$^{6.55}$, this binding mode lacks stable polar contacts, implying a relatively low affinity. Estimated by PISA,[66] the free energy of dissociation falls between 1 and 2 kcal/mol for the first mode, while only being ~0 kcal/mol for the second one. This indicates that the first binding mode is more stable and probably represents the major binding mode. In addition, both simulations show little interaction of LUF with the residues in the upper region, suggesting no subtype selectivity that is in agreement with recent experiments.[30,31]

We focused on analyzing the conformational changes of AA2AR in the first simulation, since the first binding mode seems to be the major one. We observed that at ~110 ns LUF starts to approach Trp246$^{6.48}$ with heavy-atom distances as small as 3.7 Å. After about 20 ns with LUF in close proximity, Trp246$^{6.48}$ briefly changes to the intermediate rotameric state T2 for ~5 ns, followed by a sharp increase of the volume of the G-protein binding site to over 800 Å^3 (Figure S7, Supporting Information). Our simulation suggests that the phenol group in LUF interacts with Trp246$^{6.48}$, playing a role analogous to the ribose group in adenosine-derived agonists, consistent with prior experiments that changing the substitution position of the hydroxyl group or removing it affects the ligand affinity and potency.[67,68] Moreover, the ionic lock between Arg102$^{3.50}$ and Glu228$^{6.30}$ remained broken throughout the entire simulation, while the distance between TM3 and TM6 increased to 9 Å, similar to that in the active-state crystal structure and over 2 Å larger than that in our starting model built from an inactive-state crystal structure. In general, our AA2AR–LUF simulation successfully captures the known structural features of the active state, as do our other agonist-bound simulations. Further, the sequence of conformational changes is consistent with the proposed activation mechanism. Given that LUF has a low similarity to the adenosine-derived agonists, these results suggest that this mechanism might be valid for a variety of AA2AR ligands. Additionally, despite the lack of crystallographic information about how the ligand LUF binds to AA2AR, we started from reasonable guesses for binding poses and refined them using MD simulations to obtain good agreement with mutagenesis for one of the poses. These results imply that molecular dynamics simulations can play a useful role in the structure-based design of novel small molecules, as well as to predict how they modulate AA2AR activity. Therefore, our study not only provides valuable dynamic and mechanistic insight into the ligand-dependent AA2AR activation/deactivation beyond what has been found in crystal

dx.doi.org/10.1021/ja404391q | J. Am. Chem. Soc. 2013, 135, 8749–8759

structures but should also in turn facilitate the discovery of more effective and selective AA2AR ligands.

CONCLUSION

Using unbiased MD and metadynamics simulations, we have captured the distinct structural and energetic characteristics we proposed to be related to the active and inactive states of AA2AR. The different behaviors observed in agonist-bound and inverse agonist-bound simulations reveal a number of key structural elements changing in a coherent fashion during activation or deactivation. On the basis of these correlated conformational changes, we proposed a detailed mechanism, which was also supported by subsequent metadynamics simulations. Moreover, we identified three distinct regions in the ligand-binding pocket, which seem to be responsible for agonism/antagonism, affinity, and selectivity, respectively. Finally, we confirmed our findings with simulations involving a structurally distinct agonist starting from an inactive conformation of the receptor.

We believe that our study helps advance the understanding of the AA2AR molecular mechanism of action. Our simulations can distinguish the ligand-dependent activation and deactivation, regardless of whether they are started from inactive or active conformations of this receptor. One potential application of the methodology developed in this work will be to help select GPCR ligands in drug discovery. However, since the relatively high cost of large-scale simulations might currently limit such applications to a small pool of ligand candidates, we are currently developing significantly faster mixed-resolution models based on simulations from this work.

METHODS AND MODELS

We performed all-atom simulations of AA2AR complexes in a solvated membrane environment. The CHARMM force field[69] and the Desmond 3.0 package[70] were used for all simulations. Data analysis and visualization were performed in POVME,[71] VMD,[72] and Pymol.[73] The CHARMM27-cmap[69,74] and CHARMM36-lipids[75] parameter sets were used for the protein and the lipid molecules, while the TIP3P water model was used for the solvent. Parameters for the ligands were first assigned by the CGenFF program[76] and subsequently converted to templates adapted to the parameter assignment tool Viparr.[77] Viparr was then used to assign parameters for the whole system.

We built our constructs by adding the missing atoms and residues to the crystal structures and placing the resulting protein structure into a solvated membrane model. They were relaxed using a multistage protocol which has been described before.[19] Both relaxation and production runs were performed in the NPT ensemble (310 K, 1 bar, Martyna–Tobias–Klein coupling scheme) with a time step of 1 fs. The particle mesh Ewald technique was used for the electrostatic calculations. Van der Waals and short-range electrostatics were cut off at 9.0 Å. The long-ranged electrostatics was updated every third time. We only analyzed trajectories up to 500 ns in our unbiased MD simulations and 100 ns in metadynamics simulations. Further details are given in the Supporting Information.

ASSOCIATED CONTENT

Supporting Information

Details on data set and model preparation, unbiased MD simulation protocol, metadynamics simulation protocol, volume calculation of the G-protein binding site, rotameric analysis of Trp246$^{6.48}$, and comparison of R-LUF simulation and mutagenesis data along with supporting tables and figures. This material is available free of charge via the Internet at http://pubs.acs.org.

AUTHOR INFORMATION

Corresponding Author

gavoth@uchicago.edu

Notes

The authors declare no competing financial interest.

ACKNOWLEDGMENTS

The authors thank Prof. Ad IJzerman from Universiteit Leiden and Drs. Ramy Farid, Dmitry Lupyan, and My Selvan from Schrödinger Inc. for helpful discussions. This work was supported by the National Institute of Health through grant R44-GM080726. All simulations were performed on Lonestar and Ranger at the Texas Advanced Computing Center (TACC).

REFERENCES

(1) Vauquelin, G.; von Mentzer, B. *G protein-coupled receptors: molecular pharmacology from academic concept to pharmaceutical research*; John Wiley & Sons: Chichester, 2007.
(2) Dorsam, R. T.; Gutkind, J. S. *Nat. Rev. Cancer* **2007**, *7*, 79.
(3) Thathiah, A.; De Strooper, B. *Nat. Rev. Neurosci.* **2011**, *12*, 73.
(4) Vassart, G.; Costagliola, S. *Nat. Rev. Endocrinol.* **2011**, *7*, 362.
(5) Rask-Andersen, M.; Almen, M. S.; Schioth, H. B. *Nat. Rev. Drug Discovery* **2011**, *10*, 579.
(6) Congreve, M.; Langmead, C. J.; Mason, J. S.; Marshall, F. H. *J. Med. Chem.* **2011**, *54*, 4283.
(7) Langmead, C. J.; Andrews, S. P.; Congreve, M.; Errey, J. C.; Hurrell, E.; Marshall, F. H.; Mason, J. S.; Richardson, C. M.; Robertson, N.; Zhukov, A.; Weir, M. *J. Med. Chem.* **2012**, *55*, 1904.
(8) Schwartz, T. W.; Frimurer, T. M.; Holst, B.; Rosenkilde, M. M.; Elling, C. E. *Annu. Rev. Pharmacol. Toxicol.* **2006**, *46*, 481.
(9) Yao, X.; Parnot, C.; Deupi, X.; Ratnala, V. R. P.; Swaminath, G.; Farrens, D.; Kobilka, B. *Nat. Chem. Biol.* **2006**, *2*, 417.
(10) Hoffmann, C.; Zurn, A.; Bunemann, M.; Lohse, M. J. *Br. J. Pharmacol.* **2008**, *153*, S358.
(11) Ambrosio, M.; Zürn, A.; Lohse, M. J. *Neuropharmacology* **2011**, *60*, 45.
(12) Altenbach, C.; Yang, K.; Farrens, D. L.; Farahbakhsh, Z. T.; Khorana, H. G.; Hubbell, W. L. *Biochemistry* **1996**, *35*, 12470.
(13) Trincavelli, M. L.; Daniele, S.; Martini, C. *Curr. Top. Med. Chem.* **2010**, *10*, 860.
(14) Crozier, P. S.; Stevens, M. J.; Woolf, T. B. *Proteins* **2007**, *66*, 559.
(15) Bhattacharya, S.; Hall, S. E.; Vaidehi, N. *J. Mol. Biol.* **2008**, *382*, 539.
(16) Vanni, S.; Neri, M.; Tavernelli, I.; Rothlisberger, U. *J. Mol. Biol.* **2010**, *397*, 1339.
(17) Dror, R. O.; Arlow, D. H.; Maragakis, P.; Mildorf, T. J.; Pan, A. C.; Xu, H. F.; Borhani, D. W.; Shaw, D. E. *Proc. Natl. Acad. Sci. U.S.A.* **2011**, *108*, 18684.
(18) Goetz, A.; Lanig, H.; Gmeiner, P.; Clark, T. *J. Mol. Biol.* **2011**, *414*, 611.
(19) Lyman, E.; Higgs, C.; Kim, B.; Lupyan, D.; Shelley, J. C.; Farid, R.; Voth, G. A. *Structure* **2009**, *17*, 1660.
(20) Rodriguez, D.; Pinerio, A.; Gutierrez-de-Teran, H. *Biochemistry* **2011**, *50*, 4194.
(21) Lee, J. Y.; Lyman, E. *Biophys. J.* **2012**, *102*, 2114.
(22) Lee, J. Y.; Lyman, E. *J. Am. Chem. Soc.* **2012**, *134*, 16512.
(23) Bartfai, T.; Benovic, J. L.; Bockaert, J.; Bond, R. A.; Bouvier, M.; Christopoulos, A.; Civelli, O.; Devi, L. A.; George, S. R.; Inui, A.; Kobilka, B.; Leurs, R.; Neubig, R.; Pin, J. P.; Quirion, R.; Roques, B. P.; Sakmar, T. P.; Seifert, R.; Stenkamp, R. E.; Strange, P. G. *Nat. Rev. Drug Discovery* **2004**, *3*, 574.
(24) Richardson, P. J.; Kase, H.; Jenner, P. G. *Trends Pharmacol. Sci.* **1997**, *18*, 338.
(25) Harrison, C. *Nat. Rev. Drug Discovery* **2008**, *7*, 722.

(26) Piirainen, H.; Ashok, Y.; Nanekar, R. T.; Jaakola, V. P. *Biochim. Biophys. Acta, Biomembr.* **2011**, *1808*, 1233.
(27) Shook, B. C.; Rassnick, S.; Wallace, N.; Crooke, J.; Ault, M.; Chakravarty, D.; Barbay, J. K.; Wang, A.; Powell, M. T.; Leonard, K.; Alford, V.; Scannevin, R. H.; Carroll, K.; Lampron, L.; Westover, L.; Lim, H.-K.; Russell, R.; Branum, S.; Wells, K. M.; Damon, S.; Youells, S.; Li, X.; Beauchamp, D. A.; Rhodes, K.; Jackson, P. F. *J. Med. Chem.* **2012**, *55*, 1402.
(28) Kulisevsky, J.; Poyurovsky, M. *Eur. Neurol.* **2012**, *67*, 4.
(29) Dore, A. S.; Robertson, N.; Errey, J. C.; Ng, I.; Hollenstein, K.; Tehan, B.; Hurrell, E.; Bennett, K.; Congreve, M.; Magnani, F.; Tate, C. G.; Weir, M.; Marshall, F. H. *Structure* **2011**, *19*, 1283.
(30) Lane, J. R.; Klaasse, E.; Lin, J.; van Bruchem, J.; Beukers, M. W.; Ijzerman, A. P. *Biochem. Pharmacol.* **2010**, *80*, 1180.
(31) Lane, J. R.; Herenbrink, C. K.; van Westen, G. J. P.; Spoorendonk, J. A.; Hoffmann, C.; Ijzerman, A. P. *Mol. Pharmacol.* **2012**, *81*, 475.
(32) Ballesteros, J. A.; Weinstein, H. *Methods Neurosci.* **1995**, *25*, 366.
(33) Visiers, I.; Braunheim, B. B.; Weinstein, H. *Protein Eng.* **2000**, *13*, 603.
(34) Ballesteros, J. A.; Weinstein, H. *Biophys. J.* **1992**, *62*, 107.
(35) Sankararamakrishnan, R.; Sansom, M. S. P. *Biopolymers* **1994**, *34*, 1647.
(36) Xu, F.; Wu, H. X.; Katritch, V.; Han, G. W.; Jacobson, K. A.; Gao, Z. G.; Cherezov, V.; Stevens, R. C. *Science* **2011**, *332*, 322.
(37) Jaakola, V. P.; Griffith, M. T.; Hanson, M. A.; Cherezov, V.; Chien, E. Y. T.; Lane, J. R.; Ijzerman, A. P.; Stevens, R. C. *Science* **2008**, *322*, 1211.
(38) Rasmussen, S. G. F.; Choi, H. J.; Fung, J. J.; Pardon, E.; Casarosa, P.; Chae, P. S.; DeVree, B. T.; Rosenbaum, D. M.; Thian, F. S.; Kobilka, T. S.; Schnapp, A.; Konetzki, I.; Sunahara, R. K.; Gellman, S. H.; Pautsch, A.; Steyaert, J.; Weis, W. I.; Kobilka, B. K. *Nature* **2011**, *469*, 175.
(39) Cherezov, V.; Rosenbaum, D. M.; Hanson, M. A.; Rasmussen, S. G. F.; Thian, F. S.; Kobilka, T. S.; Choi, H. J.; Kuhn, P.; Weis, W. I.; Kobilka, B. K.; Stevens, R. C. *Science* **2007**, *318*, 1258.
(40) Scheerer, P.; Park, J. H.; Hildebrand, P. W.; Kim, Y. J.; Krauss, N.; Choe, H. W.; Hofmann, K. P.; Ernst, O. P. *Nature* **2008**, *455*, 497.
(41) Rasmussen, S. G. F.; DeVree, B. T.; Zou, Y. Z.; Kruse, A. C.; Chung, K. Y.; Kobilka, T. S.; Thian, F. S.; Chae, P. S.; Pardon, E.; Calinski, D.; Mathiesen, J. M.; Shah, S. T. A.; Lyons, J. A.; Caffrey, M.; Gellman, S. H.; Steyaert, J.; Skiniotis, G.; Weis, W. I.; Sunahara, R. K.; Kobilka, B. K. *Nature* **2011**, *477*, 549.
(42) Ibrisimovic, E.; Drobny, H.; Yang, Q.; Höfer, T.; Boehm, S.; Nanoff, C.; Schicker, K. *Purinergic Signalling* **2012**, *8*, 677.
(43) Klinger, M.; Kuhn, M.; Just, H.; Stefan, E.; Palmer, T.; Freissmuth, M.; Nanoff, C. *Naunyn-Schmiedeberg's Arch. Pharmacol.* **2002**, *366*, 287.
(44) Vilardaga, J.-P.; Bunemann, M.; Krasel, C.; Castro, M.; Lohse, M. J. *Nat. Biotechnol.* **2003**, *21*, 807.
(45) Vilardaga, J.-P.; Steinmeyer, R.; Harms, G. S.; Lohse, M. J. *Nat. Chem. Biol.* **2005**, *1*, 25.
(46) Yao, X. J.; Parnot, C.; Deupi, X.; Ratnala, V. R. P.; Swaminath, G.; Farrens, D.; Kobilka, B. *Nat. Chem. Biol.* **2006**, *2*, 417.
(47) Ballesteros, J. A.; Jensen, A. D.; Liapakis, G.; Rasmussen, S. G. F.; Shi, L.; Gether, U.; Javitch, J. A. *J. Biol. Chem.* **2001**, *276*, 29171.
(48) Ahuja, S.; Hornak, V.; Yan, E. C. Y.; Syrett, N.; Goncalves, J. A.; Hirshfeld, A.; Ziliox, M.; Sakmar, T. P.; Sheves, M.; Reeves, P. J.; Smith, S. O.; Eilers, M. *Nat. Struct. Mol. Biol.* **2009**, *16*, 168.
(49) Zhu, X.; Lopes, P. E. M.; Shim, J.; MacKerell, A. D. *J. Chem. Inf. Model.* **2012**, *52*, 1559.
(50) Sakmar, T. P.; Menon, S. T.; Marin, E. P.; Awad, E. S. *Annu. Rev. Biophys. Biomol. Struct.* **2002**, *31*, 443.
(51) Provasi, D.; Artacho, M. C.; Negri, A.; Mobarec, J. C.; Filizola, M. *PLoS Comput. Biol.* **2011**, *7*, e1002193.
(52) Shan, J.; Khelashvili, G.; Mondal, S.; Mehler, E. L.; Weinstein, H. *PLoS Comput. Biol.* **2012**, *8*, e1002473.
(53) Selent, J.; Sanz, F.; Pastor, M.; De Fabritiis, G. *PLoS Comput. Biol.* **2010**, *6*, e1000884.
(54) Bonomi, M.; Barducci, A.; Parrinello, M. *J. Comput. Chem.* **2009**, *30*, 1615.
(55) Zhukov, A.; Andrews, S. P.; Errey, J. C.; Robertson, N.; Tehan, B.; Mason, J. S.; Marshall, F. H.; Weir, M.; Congreve, M. *J. Med. Chem.* **2011**, *54*, 4312.
(56) Jaakola, V. P.; Lane, J. R.; Lin, J. Y.; Katritch, V.; Ijzerman, A. P.; Stevens, R. C. *J. Biol. Chem.* **2010**, *285*, 13032.
(57) Lebon, G.; Warne, T.; Edwards, P. C.; Bennett, K.; Langmead, C. J.; Leslie, A. G. W.; Tate, C. G. *Nature* **2011**, *474*, 521.
(58) Jiang, Q.; Van Rhee, A. M.; Kim, J.; Yehle, S.; Wess, J.; Jacobson, K. A. *Mol. Pharmacol.* **1996**, *50*, 512.
(59) Kim, J.; Wess, J.; van Rhee, A. M.; Schöneberg, T.; Jacobson, K. A. *J. Biol. Chem.* **1995**, *270*, 13987.
(60) Jiang, Q.; Lee, B. X.; Glashofer, M.; van Rhee, A. M.; Jacobson, K. A. *J. Med. Chem.* **1997**, *40*, 2588.
(61) Kim, J.; Jiang, Q.; Glashofer, M.; Yehle, S.; Wess, J.; Jacobson, K. A. *Mol. Pharmacol.* **1996**, *49*, 683.
(62) Xu, F.; Stevens, R. C. *Structure* **2011**, *19*, 1204.
(63) Ongini, E.; Dionisotti, S.; Gessi, S.; Irenius, E.; Fredholm, B. B. *Naunyn-Schmiedeberg's Arch. Pharmacol.* **1999**, *359*, 7.
(64) Klotz, K. N.; Hessling, J.; Hegler, J.; Owman, C.; Kull, B.; Fredholm, B. B.; Lohse, M. J. *Naunyn-Schmiedeberg's Arch. Pharmacol.* **1998**, *357*, 1.
(65) Congreve, M.; Andrews, S. P.; Doré, A. S.; Hollenstein, K.; Hurrell, E.; Langmead, C. J.; Mason, J. S.; Ng, I. W.; Tehan, B.; Zhukov, A.; Weir, M.; Marshall, F. H. *J. Med. Chem.* **2012**, *55*, 1898.
(66) Krissinel, E.; Henrick, K. *J. Mol. Biol.* **2007**, *372*, 774.
(67) Beukers, M. W.; Chang, L. C. W.; von Frijtag Drabbe Künzel, J. K.; Mulder-Krieger, T.; Spanjersberg, R. F.; Brussee, J.; Ijzerman, A. P. *J. Med. Chem.* **2004**, *47*, 3707.
(68) Guo, D.; Mulder-Krieger, T.; IJzerman, A. P.; Heitman, L. H. *Br. J. Pharmacol.* **2012**, *166*, 1846.
(69) MacKerell, A. D.; Bashford, D.; Bellott, M.; Dunbrack, R. L.; Evanseck, J. D.; Field, M. J.; Fischer, S.; Gao, J.; Guo, H.; Ha, S.; Joseph-McCarthy, D.; Kuchnir, L.; Kuczera, K.; Lau, F. T. K.; Mattos, C.; Michnick, S.; Ngo, T.; Nguyen, D. T.; Prodhom, B.; Reiher, W. E.; Roux, B.; Schlenkrich, M.; Smith, J. C.; Stote, R.; Straub, J.; Watanabe, M.; Wiórkiewicz-Kuczera, J.; Yin, D.; Karplus, M. *J. Phys. Chem. B* **1998**, *102*, 3586.
(70) Bowers, K. J.; Chow, E.; Xu, H.; Dror, R. O.; Eastwood, M. P.; Gregersen, B. A.; Klepeis, J. L.; Kolossvary, I.; Moraes, M. A.; Sacerdoti, F. D.; Salmon, J. K.; Shan, Y.; Shaw, D. E. In *Proceedings of the 2006 ACM/IEEE conference on Supercomputing*; ACM: Tampa, FL, 2006; p 84.
(71) Durrant, J. D.; de Oliveira, C. A.; McCammon, J. A. *J. Mol. Graphics Modell.* **2011**, *29*, 773.
(72) Humphrey, W.; Dalke, A.; Schulten, K. *J. Mol. Graphics Modell.* **1996**, *14*, 33.
(73) *The PyMOL Molecular Graphics System*, version 1.5.0.4; Schrödinger, LLC.
(74) Mackerell, A. D.; Feig, M.; Brooks, C. L. *J. Comput. Chem.* **2004**, *25*, 1400.
(75) Klauda, J. B.; Venable, R. M.; Freites, J. A.; O'Connor, J. W.; Tobias, D. J.; Mondragon-Ramirez, C.; Vorobyov, I.; MacKerell, A. D., Jr.; Pastor, R. W. *J. Phys. Chem. B* **2010**, *114*, 7830.
(76) Vanommeslaeghe, K.; Hatcher, E.; Acharya, C.; Kundu, S.; Zhong, S.; Shim, J.; Darian, E.; Guvench, O.; Lopes, P.; Vorobyov, I.; MacKerell, A. D. *J. Comput. Chem.* **2010**, *31*, 671.
(77) *Desmond Molecular Dynamics System*, version 3.0; D. E. Shaw Research: New York, 2011. *Maestro-Desmond Interoperability Tools*, version 3.0; Schrödinger: New York, 2011.